



## Article

# Fractal Characteristics and Microstructure of Coal with Impact of Starch-Polymerized Aluminum Sulfate Fracturing Fluids

Feng Cai <sup>1,2,\*</sup> , Qian Zhang <sup>1,2</sup> and Lingling Yang <sup>1,2,3</sup>

<sup>1</sup> State Key Laboratory of Mining Response and Disaster Prevention and Control in Deep Coal Mines, Anhui University of Science and Technology, Huainan 232001, China; 2022100015@aust.edu.cn (Q.Z.); yll@htc.edu.cn (L.Y.)

<sup>2</sup> School of Safety Science and Engineering, Anhui University of Science and Technology, Huainan 232001, China

<sup>3</sup> Department of Biotechnology, Hefei Technology College, Hefei 238000, China

\* Correspondence: fcai@aust.edu.cn

**Abstract:** The degree of irregularity and complexity of the pore structure are comprehensively reflected in the fractal dimension. The porosity of coal was determined by its fractal dimension, where a larger dimension indicates a lower porosity. Fractal theory and the Frenkel–Halsey–Hill (FHH) model were applied to explore the variation rules of concentration on functional groups and pore structure in this study. Combined with infrared spectroscopy (FTIR) and low-temperature nitrogen adsorption, a starch-polymerized aluminum sulfate composite fracturing fluid was prepared, which plays an important role in methane adsorption and permeability of coal samples. The test results showed that, compared with the original coal, the pore volume and specific surface area of each group of coal samples were reduced, the average pore diameter was initially enlarged and then declined, and fractal dimension  $D_1$  dropped by 5.4% to 15.4%, while fractal dimension  $D_2$  gained 1.2% to 7.9%. Moreover, the nitrogen adsorption of each group of coal samples was obviously lower than the original coal, and the concentration of starch-polymerized aluminum sulfate solution existed at a critical optimal concentration for the modification of the coal samples, and the nitrogen adsorption reached a minimum value of  $0.6814 \text{ cm}^3/\text{g}$  at a concentration of 10%. The novel composite solution prepared by the combination of starch and flocculant in this paper enhanced the permeability of the coal seam, which is of great significance in improving the efficiency of coalbed methane mining.

**Keywords:** coalbed methane; starch-polymerized aluminum sulfate solution; functional group; pore structure; fractal dimension



**Citation:** Cai, F.; Zhang, Q.; Yang, L. Fractal Characteristics and Microstructure of Coal with Impact of Starch-Polymerized Aluminum Sulfate Fracturing Fluids. *Fractal Fract.* **2024**, *8*, 228. <https://doi.org/10.3390/fractalfract8040228>

Academic Editor: Zine El Abidine Fellah

Received: 3 February 2024

Revised: 26 March 2024

Accepted: 10 April 2024

Published: 15 April 2024



**Copyright:** © 2024 by the authors. Licensee MDPI, Basel, Switzerland. This article is an open access article distributed under the terms and conditions of the Creative Commons Attribution (CC BY) license (<https://creativecommons.org/licenses/by/4.0/>).

## 1. Introduction

China's coal reservoirs tend to be characterized by high gas, low permeability, difficulty in extraction and other characteristics. As a kind of clean energy, gas can not only significantly contribute to the optimization of China's energy structure but is also a leading cause of coal and gas protrusion. Consequently, achieving efficient gas operation is of great importance for reducing carbon emissions, alleviating environmental pressure, reducing gas catastrophes, and effectively improving the permeability of coal seams, which constitutes the crucial factor in cracking the low efficiency of gas extraction [1–4]. Hydraulic fracturing possesses the outstanding advantages of a wide scope of application, simple process and remarkable technical effect, and it is an important technical means to strengthen the effect of gas pre-pumping in low-permeability coal beds. Fracturing fluid, as an additive in the hydraulic fracturing process, improves the pore structure and gas desorption effect of coal seams remarkably, thus enhancing the efficiency of gas extraction.

Recently, extensive research has been carried out on the chemical structure modification of coal using fracturing fluids, providing an important reference for the choice of fracturing fluids. Xi et al. [5] examined the chemical structure of coal treated with

an ionic solution using infrared (FTIR) spectroscopy, and analysis showed that the ionic solution increased the oxygen content of the functional groups in the coal samples. Wang et al. [6] carried out a study of the functional groups in coal treated with tetrahydrofuran (THF) and  $\text{CH}_3\text{CH}_2\text{OH}$  and found that both aromatic and aliphatic functional groups were significantly reduced as a result of dissolution. Zhao et al. [7] demineralized coal using a sequential dilute hydrochloric acid, hydrofluoric acid, and hydrochloric acid leach method. It was observed that the quantity of carboxylic acid, phenolic hydroxyl group and ether oxygen increased, the amount of aliphatic ring decreased, and the length of aliphatic chain was shortened, proving that acidic solvents affect the molecular structure of coal. Liu et al. [8] studied the influence of composite solvents on the carbon structure in coal and revealed that pyridine (PY) and THF composite solvents could increase the ring size and polycondensation degree of aromatic hydrocarbons. Zhao et al. [9] pointed out, in a study on the impact of different ionic liquid concentrations on the molecular structure of lignite, that with the increase in ionic concentration, the aromaticity increases and the molecular structure becomes more compact. Through FTIR, the mercury injection method (MIP), X-ray diffraction (XRD) and other methods, Wang et al. [10] determined that the best improvement of the functional groups of coal was achieved with a hydrochloric acid content of 3% to 5%.

Coal is a porous material with a very diverse pore structure, mainly divided into micropores, mesopores and macropores. It is commonly recognized that micropores control the adsorption capacity of gases, and the larger pores determine the flow capacity of gases in coal. Recent research [11] has demonstrated that gas diffusion in a porous medium is significantly influenced by the pore structure. Fractal theory offers a useful technique for examining the way in which complex pore structures affect diffusion. Ni et al. [12] investigated a modified solution of nitric acid via the low-temperature nitrogen adsorption method, finding that the pore reaming effect was evident. Wang et al. [13] adopted the distribution characteristics of pore structures using the low-temperature nitrogen adsorption method and found that a mixed acid solution can improve shale pore connectivity and greatly reduce the specific surface area and volume of the pores. Yang et al. [14] examined the effect of SOMs on coal matrix pores, indicating that SOMs can promote coal and gas outbursts. Injection of THF, NMP, acetone and toluene can also remove soluble molecules and form new cracks and pores [15].

The above studies focused on the modification of coal samples using acidic and organic solvent solutions to investigate their effects on the microstructure and chemical structure of coal. However, chemical solutions such as acidic and organic solvents are poisonous and highly corrosive, causing environmental pollution, harming human health, and damaging instruments in the process of use. It is therefore crucial to explore an effective, non-toxic, non-corrosive, and low-cost fracturing fluid to improve the permeability of coal seams. To date, the application of organic and inorganic polymer flocculant composites in the field of wastewater settling has been widely studied [16–18]. Among these studies, soluble starch solution and phenolic components in the chemical structure exhibit better flocculation effects, while polymerized aluminum sulfate flocculant solution and minerals in coal yield different flocculation results. Meanwhile, soluble starch and flocculant showed high stability and environmental friendliness [19–21]. Compounding the two enhances the flocculation activity and also allows the flocculation products and detritus to be degraded. The clean fracturing fluid obtained after compounding is able to perform effectively in improving the microstructure of coal, thus increasing the efficiency of gas extraction.

In summary, the aim of this study is to investigate the impact of different concentrations of a new composite solution on the microstructure and fractal characteristics of coal. Through Fourier transform infrared spectroscopy and low-temperature nitrogen adsorption experiments, fractal theory was applied to analyze the variation rules of functional groups and pore structures that are affected by different concentrations of composite solutions on methane adsorption and permeability of coal samples [22–24]. The results of this study help to dramatically enhance the gas extraction rate, thereby decreasing or eliminating gas

disasters, and ultimately provide a theoretical basis for the safe and efficient extraction of methane from coal mines.

## 2. Experiments

### 2.1. Material and Methods

The solution of soluble starch and polymerized aluminum sulfate was selected and mixed based on a 1:1 mass ratio, and the solution of aluminum sulfate polymerized with starch at concentrations of 1%, 5%, 10%, 15%, and 20% was prepared.

In this experiment, gas coal from the Yunnan Yuwang coal mine was selected; the basic parameters of the coal samples are shown in Table 1. The core sample was crushed and 0.178 to 0.25 mm of coal was sifted into the prepared starch–flocculant solution for 48 h to make full contact with the solution. The treated coal samples were labeled, cleaned, filtered and placed in a thermostatic vacuum dryer at 50 °C to dry to a constant weight before being sealed for use. The technical route of the study is shown in Figure 1.

**Table 1.** The basic parameters of the coal samples.

Type	$M_{ad}/\%$	$V_{daf}/\%$	$A_{ad}/\%$	$F_{Cad}/\%$
raw coal	3.38	9.91	9.86	81.2

Annotations:  $M_{ad}$  is the moisture content under air-drying conditions,  $A_{ad}$  is the ash content under air-drying conditions,  $V_{daf}$  is the volatile matter content under air-drying conditions, and  $F_{Cad}$  is the fixed carbon content under air-drying conditions.

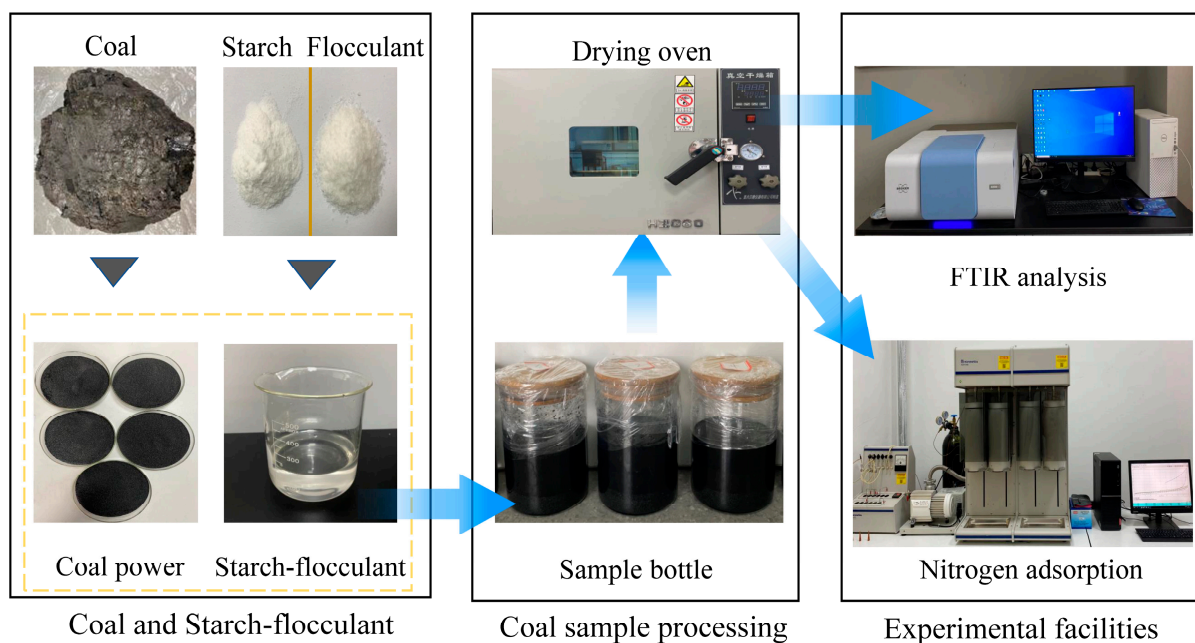


**Figure 1.** Technical route.

### 2.2. Experimental Steps

#### 2.2.1. FTIR Measurements

Measures of  $1 \pm 0.01$  mg of coal particles and  $200 \pm 0.01$  mg of potassium bromide powder were mixed uniformly and ground for 120 s and then pressed into 0.1–1 mm slices using the tablet pressing method. The test was carried out using a Fourier-transform infrared spectrometer from Bruker, Germany, with a scanning range of  $4000\text{--}400\text{ cm}^{-1}$  and a scanning resolution of  $4\text{ cm}^{-1}$ , and the number of scans was 32. To minimize experimental errors, three scanning experiments were carried out for each coal sample.

## 2.2.2. Low-Temperature N<sub>2</sub> Adsorption

The coal samples were degassed under vacuum at 135 °C using an America Micromeritics ASAP 2460 BET analyzer (McMorrettick Instruments Co., Shanghai, China). After air and impurities were completely removed from the coal samples, the samples were placed in 77 K liquid nitrogen for testing, and the nitrogen adsorption and detachment isotherms were obtained with the relative pressures ( $P/P_0$ ) in the range of 0.001–0.995.

## 3. Results and Discussion

### 3.1. FTIR Analysis

To analyze the complex functional group distribution of coal, the FTIR spectra were divided into four parts, as shown in Figure 2. These parts included hydroxyl structures in the 3000–3600 cm<sup>-1</sup> range, aliphatic hydrocarbon structures in the 2800–3000 cm<sup>-1</sup> range [25], oxygenated functional groups in the 1000–1800 cm<sup>-1</sup> range, and aromatic hydrocarbon structures in the 700–900 cm<sup>-1</sup> range [26], where DX0 is raw coal and DX1, DX2, DX3, DX4, and DX5 are coal samples treated with starch-polymerized aluminum sulfate solution at concentrations of 1%, 5%, 10%, 15%, and 20%, respectively.

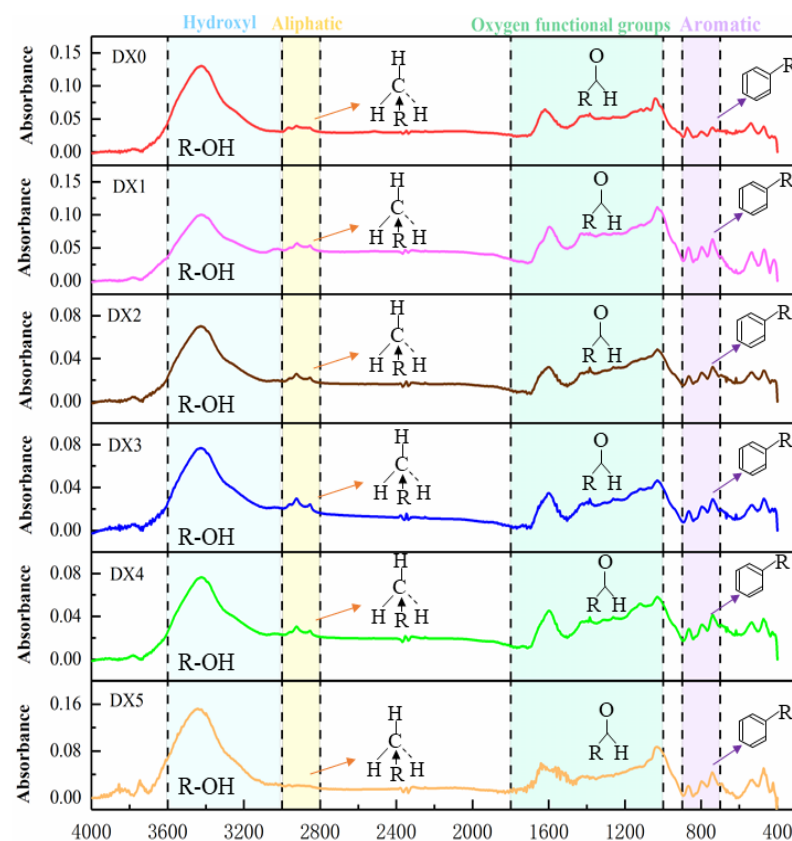


**Figure 2.** Infrared spectra of different coal samples.

The infrared spectrograms of coal samples treated with different concentrations of starch-polymerized aluminum sulfate solutions were fitted with sub-peaks. The overlapping peaks of various functional groups in coal were broken down into sub-peaks based on the Gaussian function, and their peaks and peak widths were determined. Through the qualitative and quantitative calculation of the peak area of each functional group, the structural features of the coal have been characterized.

Figure 3 and Table 2 demonstrate the FTIR peak-fit statistics and summary of the peak areas of the functional groups for each group of coal samples, respectively, which show that the hydroxyl structures of coal samples treated with different concentrations of the starch-polymerized aluminum sulfate solution were concentrated primarily in the

3000–3600  $\text{cm}^{-1}$  range. Between five and eight Gaussian peaks were fitted for the six coal samples, in which there existed stretching vibrations of the phenol compounds bonded with -OH (or -NH), aromatic nuclei CH stretching vibrations (3080–3035  $\text{cm}^{-1}$ ), and aromatic nuclei CH stretching vibrations (3080–3035  $\text{cm}^{-1}$ ). (3600–3200  $\text{cm}^{-1}$ ), and aromatic nuclear CH stretching vibrations (3080–3035  $\text{cm}^{-1}$ ). The peak area of associative hydrogen bonds decreased from 31.64 in raw coal to 11.79 in DX1 coal. With the increase in solution concentration, the starch-polymerized aluminum sulfate solution demonstrated a strong adsorption effect, broke the hydrogen bond in coal, and caused the structure of hydroxyl to gradually decline. This suggested that the action of starch-flocculant solution resulted in a change in the state of existence of hydroxyl functional groups, which, in turn, reduced the adsorption capacity of coal for methane [27].

The aliphatic hydrocarbon structure is concentrated primarily in the 2800–3000  $\text{cm}^{-1}$  range, and between three and seven Gaussian distributions are synthesized from six coal samples, in which the aliphatic -CH<sub>2</sub>, -CH<sub>3</sub> asymmetric stretching vibration exists. The aliphatic hydrocarbon structure of the coal sample is markedly reduced compared to that of the raw coal, and the peak areas of DX3 and DX4 are reduced by 91% and 93.5%, respectively. This is due to the fact that as the concentration of starch-aluminum polymerized sulfate solution increases, the methyl hypomethyl group in aliphatic hydrocarbons is constantly being solubilized, decreasing the length of the aliphatic chain. Thus, the adsorption performance of methane in coal is weakened [28].

Oxygen-containing functional groups are concentrated in the 1000–1800  $\text{cm}^{-1}$  range, where there are aliphatic and aromatic C=O stretching vibrations (1770–1700  $\text{cm}^{-1}$ ), aromatic C=C vibrations (1645–1545  $\text{cm}^{-1}$ ), aryl-core C-C vibrations (1545–1480  $\text{cm}^{-1}$ ), asymmetric deformation vibrations of the aliphatic chains of CH<sub>3</sub>, CH<sub>2</sub> (1480–1421  $\text{cm}^{-1}$ ), CH<sub>3</sub> symmetric bending vibrations (1420–1350  $\text{cm}^{-1}$ ), C-O-C stretching vibrations of phenols, and alcohols and ethers (1300–1000  $\text{cm}^{-1}$ ). Six coal samples were proposed to synthesize between eight and eleven Gaussians. From Figure 3 and Table 2, it is evident that the peaks are numerous within this region. As the concentration of starch-polymerized aluminum sulfate solution increased, the aromatic C=O backbone vibration of DX1 increased by 56.7%, the aromatic nucleated C-C backbone vibration of DX4 decreased by 93.7%, while the aromatic nucleated C-C backbone vibration of DX5 increased by 337%. The C-O-C tensile vibrations of phenols, alcohols and ethers of all groups of coal samples presented an increasing trend, and the value of DX5 was the maximum. It is thus clear that starch-flocculant solutions affect oxygenated functional groups variably.

The aromatic hydrocarbon structures were mainly concentrated between 700 and 900  $\text{cm}^{-1}$  range, in which C-H bending vibration on the benzene ring existed, and between five and eight Gaussian distributions were proposed to be synthesized for six coal samples. The C-H bending vibration on the benzene ring displayed an upward and then downward trend but generally increased compared to the original coal. This is because the deoxygenation of the cycloalkanes in the coal leads to aromatization, which changes the degree of condensation of the aromatic hydrocarbons.

Overall, the structure of the functional groups of each group of coal samples changed significantly after treatment with different concentrations of starch-polymerized aluminum sulfate solution. The associative hydrogen bonding was reduced, the methyl hypomethyl group in the aliphatic hydrocarbons was constantly dissolved, and the aliphatic chain was destroyed, leading to a reduction in the length of the aliphatic chain. An aromatization reaction occurred between the coal molecules, and the content of oxygen-containing functional groups initially increased and then decreased, and the quantity of aromatic hydrocarbons was little altered.

Table 2. Summary of peak areas of functional groups.

Wavenumber/cm <sup>-1</sup>	Code	Samples						Characteristic Parameters
		DX0	DX1	DX2	DX3	DX4	DX5	
3600~3200	A	31.64	11.79	13.32	14.71	13.42	29.12	$I_1 = A_v(\text{CH}_2) + A_v(\text{CH}_3) + A_v(\text{CH}_2 + \text{CH}_3)/A_v(\text{C}-\text{C}) = A_C + A_G + A_H/A_E + A_F$
3080~3035	B	0.048	0.081	0.044	0.054	0.124	0.171	
3000~2800	C	0.891	0.624	0.620	0.083	0.061	0.213	
1770~1700	D	0.039	0.030	0.057	0.031	0.072	0.022	$I_2 = A_v(-\text{OH}) + A_v(\text{C}-\text{O}) + A_v(\text{C}-\text{O}-\text{C})/A_v(\text{C}-\text{C}) = A_A + A_D + A_I/A_E + A_F$
1645~1545	E	3.123	4.898	3.128	3.709	3.740	3.921	
1545~1480	F	0.167	0.047	1.670	0.086	0.011	2.243	
1480~1421	G	0.676	0.734	0.427	0.019	0.020	2.962	$I_3 = A_v(-\text{CH}) + A_v(-\text{CH})/A_v(\text{CH}_2 + \text{CH}_3) = A_B + A_J/A_C$
1420~1350	H	0.604	0.558	0.332	2.333	1.229	0.931	
1300~1000	I	1.611	1.715	1.690	2.731	2.063	3.042	
900~700	J	0.811	2.284	0.839	1.012	1.359	2.332	$I_4 = A_v(-\text{CH}) + A_v(-\text{CH})/A_v(\text{C}-\text{C}) = A_B + A_J/A_E + A_F$

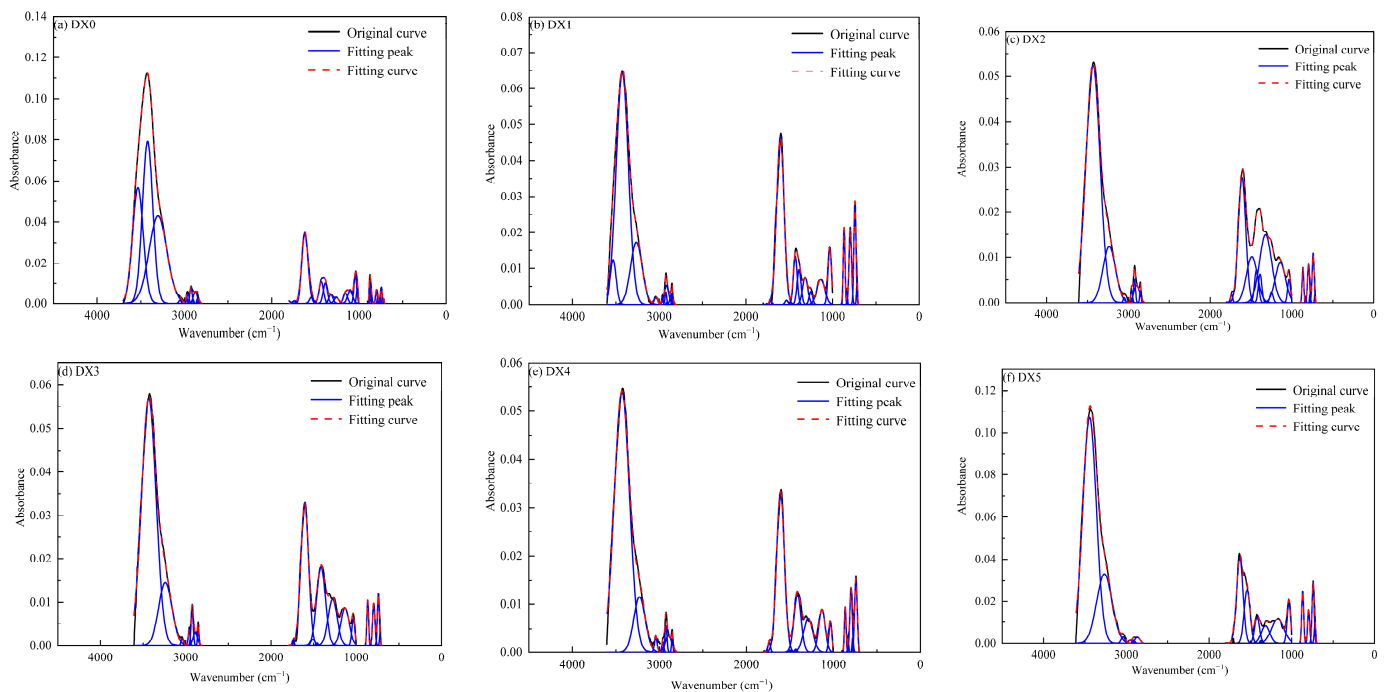
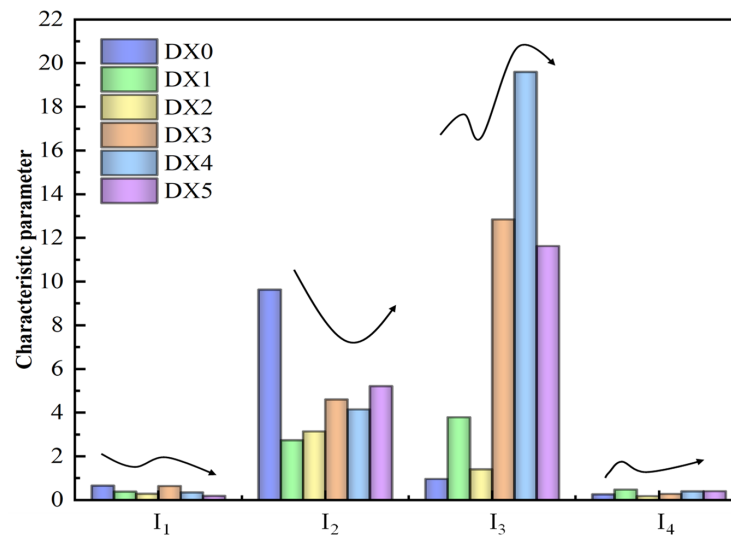


Figure 3. FTIR peak fitting statistical diagrams for different coal samples.

Using the peak areas of each attributed functional group obtained from the split-peak fitting integrals, the hydrogen-rich index  $I_1$ , oxygen-rich index  $I_2$ , aromaticity  $I_3$ , and condensation  $I_4$  were calculated using the data in Table 2, as illustrated in Figure 4. As the concentration of the polyaluminum sulfate solution of starch was increased,  $I_3$  first increased and then decreased.  $I_3$  reached a maximum value of 25.6 when the concentration of the starch-polyaluminum sulfate solution was 15% of the total. This is due to the fact that fat chain cyclization and naphthene dehydrogenation increase the degree of aromatization in the process of soaking coal. Compared to raw coal, the  $I_4$  values in DX1 coal and DX4 coal are slightly higher, indicating that the adsorption of starch-flocculant solution favors partial aromatic condensation to form certain polycyclic aromatic hydrocarbons. The overall significant decrease in  $I_2$  points to a notable correlation between oxygen-containing functional groups and the starch-polymerized aluminum sulfate solution concentration.  $I_1$  shows a fluctuating trend with increasing solution concentration, indicating a more complex change in aliphatic structure with increasing solution concentration.



**Figure 4.** Characteristic parameters of functional groups of different coal samples.

### 3.2. Pore Morphology

Coal, as a porous medium, exhibits a complex pore structure. The pore morphology in the microstructure of the coal body affects the storage and transportation characteristics of gas from coalbed methane [29]. Figure 5 shows the  $N_2$  isotherm adsorption and desorption curves of the raw and treated coals, which are type IV isotherms according to the IUPAC classification standard. There was a rapid upward trend in the adsorption of  $N_2$  in each group of coal samples when the relative pressure  $P/P_0$  was approximately 0.04, indicating capillary filling of the ultramicropores and marking the stage of adsorption of monolayers. As the relative pressure was increased, the monolayer adsorption step was converted to the multilayer adsorption and capillary condensation step. As the concentration of the starch-polymerized aluminum sulfate solution was increased, the maximum nitrogen adsorption of each treated coal sample decreased by 4.08–63.1% relative to the original coal and reached the minimum value for nitrogen adsorption in the DX3 coal. Simultaneously, the adsorption isotherm gradually slowed down; that is, the adsorption rate decreased. The adsorption capacity was lowest when the concentration of the starch-polyaluminum sulfate solution was 10%.

When  $P/P_0$  was near 0.45, the raw coal desorption curve had a steeply declining inflection point, indicating that the pores in the raw coal consisted primarily of a fine bottleneck and inkwell pores. The sudden decrease in the isotherms of the treated coal was not evident, suggesting that the pores consisted primarily of columnar pores. When  $P/P_0$  was between 0.45 and 0.95, the raw coal displayed an obvious hysteresis line, and the hysteresis area significantly diminished and approached closure as the concentration of starch-polymerized aluminum sulfate solution increased. This suggests that the internal pore size of the treated coal may be lessened and the pore connectivity improved, reaching an approximate adsorption–desorption equilibrium, which is favorable for the desorption and diffusion of methane. Hence, the effect of starch-polymerized aluminum sulfate solution modification on the pore structure was dramatic.

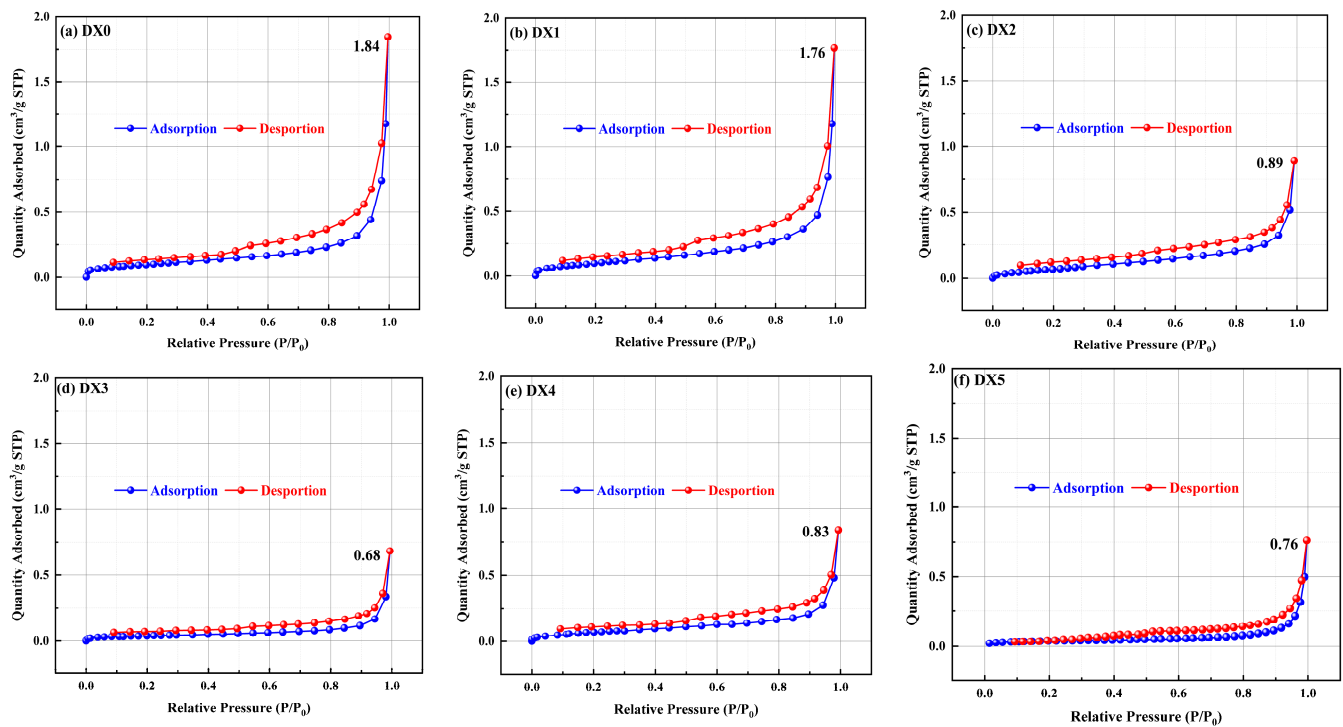


**Figure 5.** Isothermal curves of different coal samples.

### 3.3. Pore Size Distribution

Meanwhile, the pore size distribution characteristics in the microstructure of the coal body also dictate the storage and mobility of coalbed methane. Before the analysis of pore size distribution, the pore size should be categorized. In accordance with the IUPAC pore classification method, the pores are characterized as micropores (<2 nm), mesopores (2~50 nm), and macropores (>50 nm) [30]. Micropores determine the adsorption capacity of the gas, and the mode of action of coalbed methane is dominated by physical adsorption and capillary condensation. Mesopores and macropores dictate the diffusion and flow capacity of the gas; coalbed methane exists mostly as a result of seepage [31].

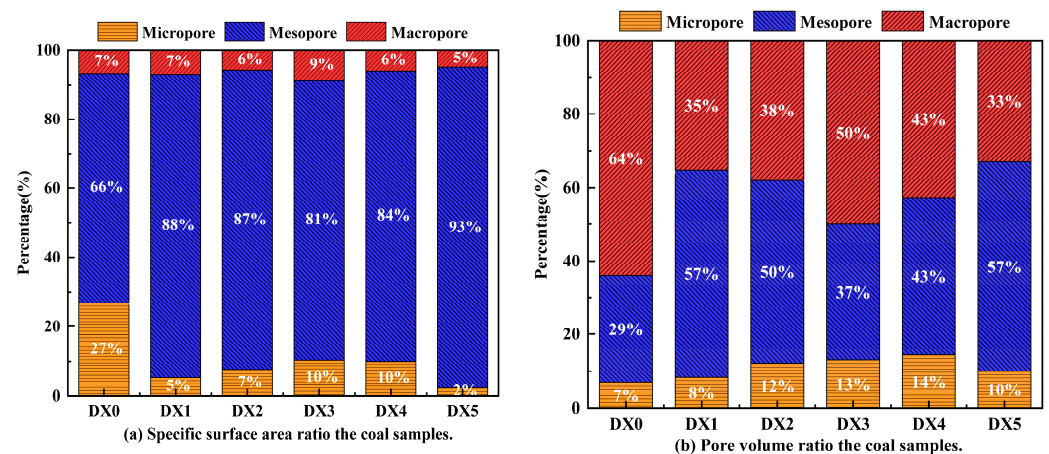
TPV (pore volume) and SSA (specific surface area) results for each coal sample pore are shown in Table 3. Compared with raw coal, the DX3 coal presented the lowest SSA of 0.01537 m<sup>2</sup>/g, while the raw coal presented the highest SSA of 0.03874 m<sup>2</sup>/g. The DX1 coal exhibited a greater SSA and lesser TPV, which was related to pore collapse owing to adsorption of the starch-aluminum polymerized sulfate solution. The SSA value of DX2 coal was less than DX5 coal, but the TPV of both coals was nearly the same, indicating that the starch-polymerized aluminum sulfate solution not only increased the volume of the micropores but also decreased the volume of the mesopores and macropores. The DX3 coal clearly demonstrated a lower volume of micropores, which is consistent with the results of nitrogen adsorption shown in Figure 5, illustrating the capacity of gas adsorption determined by the micropores. The average pore size initially increased and then decreased as the concentration of the starch-polymerized aluminum sulfate solution increased. The average pore diameter of DX3 coal reached its maximum value, which was 28.7% more than that of DX0 coal. In general, the TPV and SSA of coal samples were reduced relative to the raw coal, and the effect was most marked when the concentration of starch-polymerized aluminum sulfate solution was 10%. For further analysis of the SSA and TPV changes in the coal samples from the starch-polymerized aluminum sulfate solution, the parameters in Table 3 were plotted as percent stacking plots.

**Table 3.** Characteristic parameters of pore structure of different coal samples.

Samples	Volume ( $10^{-3}\text{cm}^3/\text{g}$ )			TPV ( $\times 10^{-3}\text{cm}^3/\text{g}$ )	SSA ( $\text{m}^2/\text{g}$ )			SSA ( $\text{m}^2/\text{g}$ )	Average Pore Size (nm)
	Micropore	Mesopore	Macropore		Micropore	Mesopore	Macropore		
DX0	0.0922	0.3468	0.7385	1.1775	0.0156	0.3859	0.0387	0.4402	18.7922
DX1	0.0980	0.6653	0.4138	1.1771	0.0288	0.4784	0.0377	0.5512	20.1077
DX2	0.0664	0.2556	0.1943	0.5163	0.0330	0.3873	0.0257	0.4534	17.4464
DX3	0.0370	0.1270	0.1727	0.3367	0.0183	0.1429	0.0153	0.1766	26.3684
DX4	0.0688	0.2070	0.2049	0.4607	0.0352	0.2917	0.0193	0.3949	17.8398
DX5	0.0525	0.2983	0.1716	0.5251	0.011	0.4584	0.0242	0.4936	23.2461

The SSA trended to be less as the concentration of starch-polymerized aluminum sulfate solution increased when the pore size was  $<2\text{ nm}$ , as shown in Figure 6, and the SSA ratio dropped from 27% for the original coal to 2% for the DX5 coal. The percentage of TPV in this pore size range fluctuated, increasing from 7% in the original coal to 13% in the DX2 coal, declining to 11% in the DX3 coal, and then reaching a maximum in DX4. Nonetheless, coal samples treated with starch-polymerized aluminum sulfate solution appeared to have no specific trend. The maximal proportions of TPV and SSA in the range of pore sizes  $<2\text{ nm}$  occur in DX4 and raw coal, respectively.

When the pore size is 2–100 nm, more than 66% of the mesopores are SSA from each coal sample group, indicating that coal SSA is predominantly dominated by mesopores. However, the proportion of mesopores and macropores in the TPV exceeds 86%, demonstrating that mesopores and macropores contributed more to TPV than micropores. As the concentration of starch-polymerized aluminum sulfate solution increased, the mesopore volume ratio increased from 29% in the original coal to 57% in the DX1 and DX5 coals, the macropore volume ratio decreased from 64% in the original coal to 33% in the DX5 coal, and the SSA ratio of mesopore and macropore increased from 73% in the original coal to 98% in the DX5 coal. This indicated that the amount of micropores in the coal samples gradually diminished with the increase in the concentration of starch-polymerized aluminum sulfate solution, thereby causing the SSA to lower. Micropores and mesopores are widely believed to offer the greatest contribution to coal SSA and TPV, but both the SSA and TPV of treated coals were reduced owing to the adsorption of starch–flocculant solution not only inducing the transformation of macropores to micropores and mesopores but also leading to the collapse of some of the macropores, thus decreasing the TPV and SSA of the coals. It was further confirmed that the starch–flocculant solution enhanced the development of mesoporous and macroporous pore structures and increased the gas transport capacity, which was conducive to the diffusion and flow of gas [32].

**Figure 6.** Percentage of parameters for different coal samples.

From the DFT model [33], the distribution of pore sizes and the cumulative volume of pores in 0–35 nm were obtained, as shown in Figure 7. It is illustrated that the size of most of the pores in each group of coal samples was between 0 and 10 nm, implying that the coal samples before and after processing were dominated by micropores and mesopores. In Figure 7a, a strong peak appeared in the 0.7–3.1 nm range, and the peak was  $0.683 \times 10^{-3} \text{ cm}^3/\text{g}\cdot\text{nm}$  at a wavelength of 0.77 nm, suggesting that more micropores were present in the 0.7–3.1 nm range, with pore sizes concentrated at 0.77 nm. As shown in Figure 7b, the pore size of the DX1 coal was concentrated in the 0.7–4.56 nm range; the peaks between 1.1 and 2.1 nm are wider, meaning that the quantity of pores increases between 1.1 and 2.1 nm. The peaks at 1.1–2.1 nm in the DX1 coal increased compared to the original coal, and peaks simultaneously emerged at 4.5 and 6.9 nm. The pore size of DX2 coal is complicated in the 0.8–5.2 nm range, with a maximum peak at 2.1 nm relative to the original coal, and peaks at 3.1, 4, and 5.3 nm, respectively, indicating that the pore space in the 0.8 to 5.3 nm range was more numerous and more concentrated. DX3 coal demonstrated high fluctuation in the 1.4–3.5 nm range, with strong narrow peaks on either side at approximately 2.3 nm. This underlines that the pores are concentrated in the 1.4–3.5 nm range. The DX4 coal peaked at 1.6 nm, and the pores were more concentrated at 0.8–5.5 nm. The DX5 coal showed a richer pore distribution in the 1.7–10.2 nm range, and multiple peaks appeared at 2.5 and 3.9 nm. Moreover, the fluctuation of each group of coal samples in 10–35 nm was minor, illustrating that the pore distribution in this range is more uniform, but the porosity quantity is less. From this, the distribution of pore sizes of coal samples was richer after treatment with starch-polymerized aluminum sulfate solution, suggesting that starch-polymerized aluminum sulfate solution dramatically enhanced the diversity of pore sizes.

In the pore size range of 0–35 nm, the maximum peak value of raw coal at 0.7 nm was  $0.0007 \text{ cm}^3/\text{g}\cdot\text{nm}$ . The reduction in the peak value of the coal samples with the increase in starch-flocculant solution concentration indicates that the molecules of the starch-flocculant solution enter the micropores of the coal, dissolve part of the organic matter, and increase the connectivity between the pores of the coal to a degree.

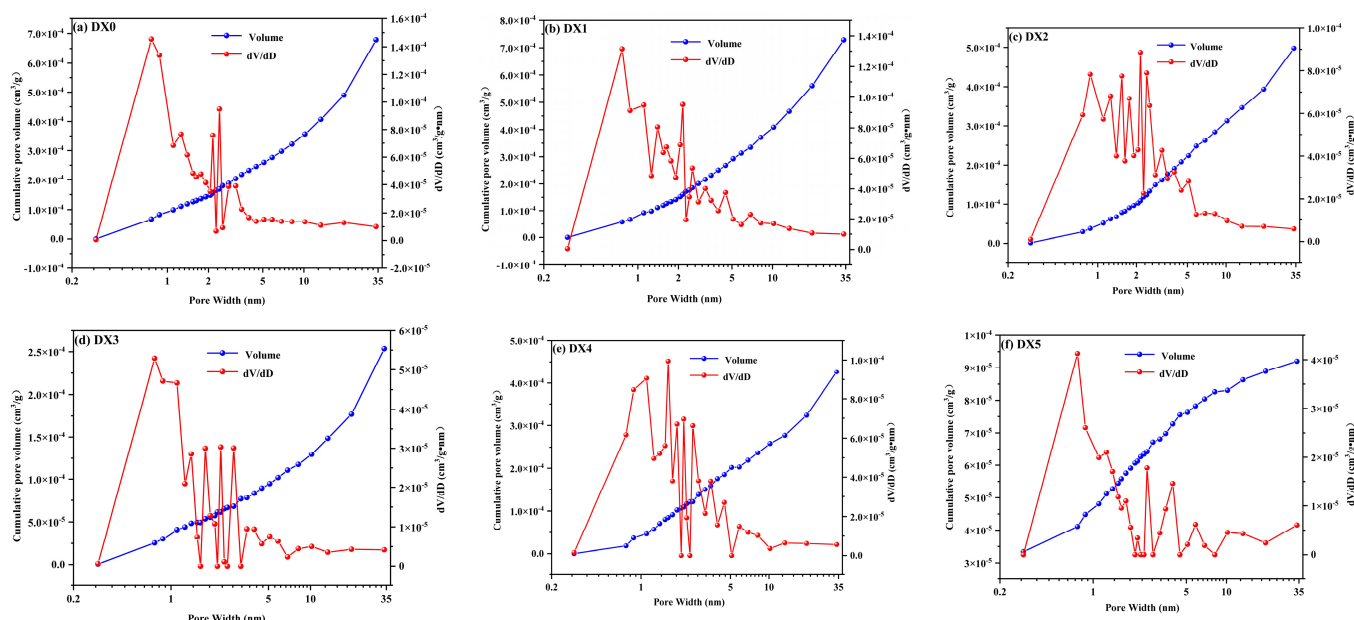


**Figure 7.** Pore size distribution and cumulative pore volume of different coal samples.

The cumulative pore volume curves of each group of coal samples varied slightly and rose gently in the 0.8–35 nm range, but the cumulative pore volume decreased progressively with the increase in the concentration of starch-polymerized aluminum sulfate solution,

which decreased by 0.03–71.4%. The results revealed that starch-polymerized aluminum sulfate solution affected the pore characteristics of coal dramatically, increasing the count of pores and lowering the pore volume.

### 3.4. Fractal Characteristics

The Brunauer–Emmett–Teller (BET) method, Frenkel–Halsey–Hill (FHH) [34,35] method, and thermodynamic methods are frequently applied to calculate the fractal dimension of solids; due to the anisotropy and complexity of the coal pore structure, the conventional fractal model cannot accurately characterize the pores. Therefore, in this paper, the Frenkel–Halsey–Hill (FHH) model is preferred to calculate the fractal dimension of coal. The equations are as follows:

$$\ln V = D \ln[\ln P/P_0] + C \quad (1)$$

where  $V$  is gas molecular volume adsorbed at equilibrium pressure, mL/g;  $D$  is a Power Law Index with a value equal to the slope of the FHH curve;  $P$  is the gas adsorption equilibrium pressure, MPa;  $P_0$  is the saturated vapor pressure of gas molecules adsorption, MPa; and  $C$  is a constant.

When the relative pressure is at  $P/P_0 < 0.5$ , the gas is adsorbed on the surface of the micropores within the coal primarily through van der Waals forces. With the relative pressure at  $P/P_0 > 0.5$ , gas adsorption depends mainly on capillary cohesion. Therefore, the fractal dimension was calculated by fitting the curve segments to characterize the pore properties of coal at different pressure stages [36]. The fractal curve is generally categorized into two stages:  $0 < P/P_0 < 0.5$  and  $0.5 < P/P_0 < 1$ . The corresponding fractal dimensions of the two stages are  $D_1$  and  $D_2$ , respectively;  $D_1$  is used to recognize the roughness of the pore surface, and  $D_2$  is used to define the complication of the pore structure. The larger the  $D$  is, the rougher the pore surface is, and the more complicated the pore structure is [37,38]. According to Eq. 1, the fractal dimension  $D$  [39–42] is derived from the slope calculation of the linear fit as shown in Figure 8 and Table 4.

**Table 4.** Fractal characterization parameters.

Samples	Fractal Dimension			
	$D_1$	$R^2$	$D_2$	$R^2$
DX0	2.4057	0.9901	2.4999	0.9966
DX1	2.2752	0.9902	2.5301	0.9984
DX2	2.0350	0.9624	2.6984	0.9854
DX3	2.4454	0.9585	2.4693	0.9888
DX4	2.1019	0.9563	2.5708	0.9867
DX5	2.6355	0.9895	2.4444	0.9839

The adjusted correlation coefficient (Table 4) for each coal sample group is above 0.95, indicating that the impacts of different concentrations of starch-polymerized aluminum sulfate solutions on the pore surface of coal are distinctly fractal in character. The  $D_1$  value of the original coal was 2.4057, and the  $D_1$  value was reduced from 5.4% to 15.4% after treatment with a solution of starch-polymerized aluminum sulfate. This indicated that the roughness of the pore surface of the coal samples was less after treatment with starch-polymerized aluminum sulfate solution, and the change was more pronounced as the concentration of starch–flocculant solution increased, which means that the starch-polymerized aluminum sulfate solution removed some of the inorganic minerals in the coal and made the surface of the pores smoother.  $D_2$  increased by 1.2–7.9% relative to the original coal after treatment with a starch–flocculant solution. As the concentration of starch–flocculant solution increased, the stronger solution absorbed the minerals in

the coal, making  $D_2$  larger. This demonstrated that the complexity of the pore structure of coal increased after starch–floculant solution treatment, and the pores became relatively uniform, which increased the connectivity of the pores. It is worth noting that the variation rules of  $D_1$  and  $D_2$  of DX3 and DX5 are different from those of other groups of coal samples. The performance of  $D_1$  increases and  $D_2$  decreases, that is, when the concentration of starch-polymerized aluminum sulfate solution is 10% and 15%, the reaction between the solution and the mineral makes the pore surface rougher and reduces the complexity of the pore structure of the coal samples, which is consistent with the findings of the nitrogen adsorption–desorption curves and the pore size distribution. Overall, the physical microstructure of the pores underwent a smooth to rough to smooth process as the concentration of the starch–floculant solution was increased.

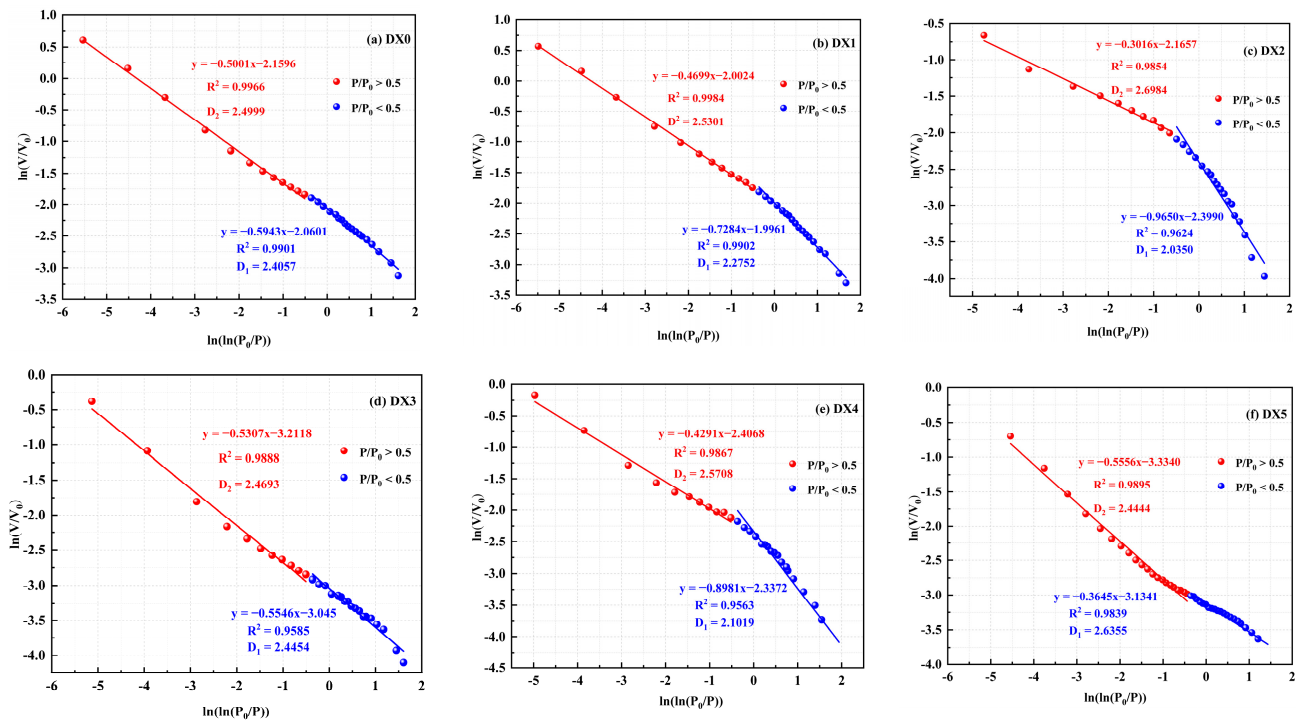


**Figure 8.** Fractal parameters of different coal samples.

### 3.5. Mechanism of Starch-Polymerized Aluminum Sulfate Solution on Coal

The purpose of the study was to probe the variation rules of functional groups and the pore structure of coal under the action of different concentrations of starch-polymerized aluminum sulfate solutions that were important to the methane adsorption and permeability of the coal samples. According to the results, the mechanism of action of starch-polymerized aluminum sulfate solution on coal was summarized, as shown in Figure 9. Small molecules of soluble organic compounds and inorganic minerals exist among the pores of the raw coal. In the solution handling process, the starch–floculant solution penetrates into the pores of the coal, dissolves some of the soluble compounds, and creates new cracks. It thus diminishes the pore volume and specific surface area of the coal, eroding the adsorption capacity of the gas. Then, the connected hydrogen bonds in the coal were visibly minimized and the fat chains were disrupted, leading to increased aromatization. Upon separation of the solution from the coal, the flocculation of the starch–floculant solution sorbed some of the insoluble small molecules out of the coal, expanding the pore channels and leading to improved connectivity between the clefts.

Meanwhile, the adsorption amount of nitrogen in coal samples decreased to differing extents after treatment with starch-polymerized aluminum sulfate solution (Figure 10). With the increase in the concentration of starch-polymerized aluminum sulfate solution, the adsorption amount of nitrogen on coal samples demonstrated an “inverted N”-type

decreasing trend, and the adsorption amount of nitrogen on coal samples was minimal in the DX3 coal samples:  $0.6814 \text{ cm}^3/\text{g}$ . This is due to the starch-polymerized aluminum sulfate solution and coal particles being in contact, causing partial swelling of soluble macromolecules. The molecular volume expands outward and squeezes the original pores, causing a reduction in the volume of micropores, thus reducing the degree of adsorption of nitrogen. With the increase in the concentration of starch-polymerized aluminum sulfate solution, the swelling phenomenon is clearer; the best effect is noted when the concentration of starch-polymerized aluminum sulfate solution is 10%.

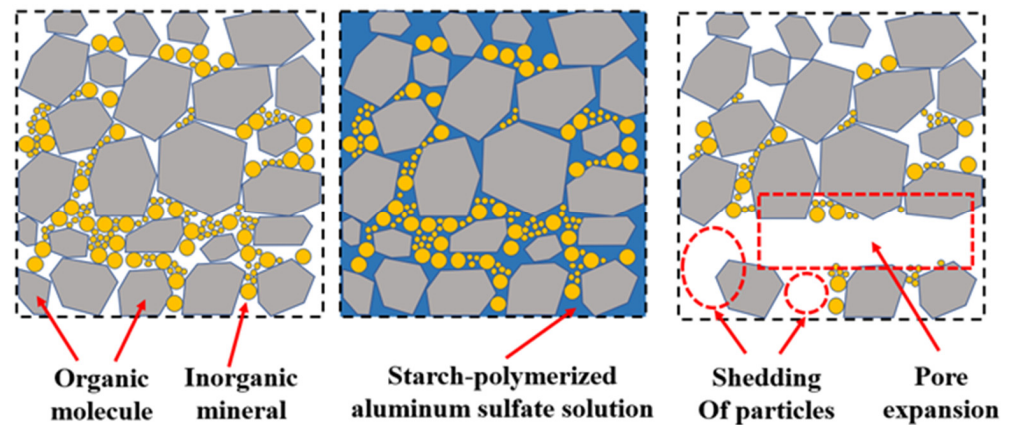


Figure 9. Mechanism of starch-polymerized aluminum sulfate solution on coal.

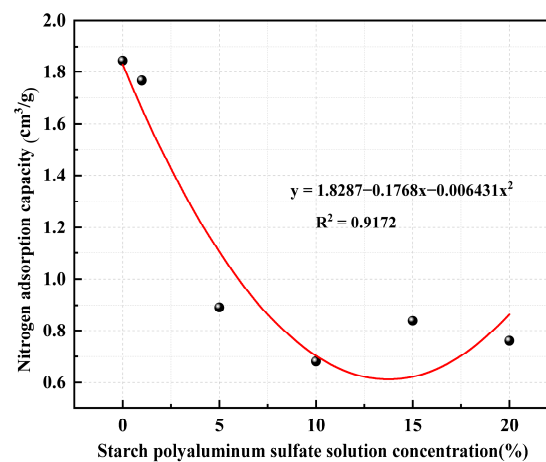


Figure 10. Nitrogen adsorption capacity of different coal samples.

#### 4. Conclusions

In this study, through Fourier transform infrared spectroscopy (FTIR) and low-temperature nitrogen adsorption experiments, fractal theory was implemented to analyze the changing rules of functional groups and pore structures in the effect of different concentrations of composite solutions on the methane adsorption and permeability of coal samples. The results of the study are expected to provide theoretical support for the optimization of fracturing fluids in the hydraulic fracturing process. The main findings are as follows:

- (1) The structure of the functional groups dramatically changed as the concentration of starch-polymerized aluminum sulfate composite solution increased. Contracted hydrogen bonds were markedly minimized. Moreover, the methyl hypromellose was constantly dissolved, resulting in the shortening of the aliphatic chain length. The content of oxygen-containing functional groups initially increased and then decreased, and the quantity of aromatic hydrocarbons exhibited no obvious alteration, which was favorable to the desorption of gas.

- (2) With the increase in starch-polymerized aluminum sulfate solution concentration, the TPV and SSA of all treated coal samples declined, and the average pore size increased and then decreased, which particularly affected the pore structure of DX3 coal. This indicates that the adsorption effect of the starch–flocculant solution induces the transformation of macropores to micropores and mesopores, which is conducive to gas extraction.
- (3) Fractal dimension  $D_1$  decreased by 5.4–15.4% and fractal dimension  $D_2$  increased by 1.2~7.9% after treatment with starch-polymerized aluminum sulfate solution. As the concentration of starch–flocculant solution increased, the solution adsorption of minerals in the coal became stronger, which caused the pore structure of the coal to become more complex, thus increasing the connectivity of the pores.
- (4) The nitrogen adsorption of each group of coal samples was reduced, and it was clearly less than that of the original coal. With the increase in starch–flocculant solution concentration, the adsorption of nitrogen by coal displayed an “inverted N” trend and arrived at the minimum value of nitrogen adsorption of  $0.6814 \text{ cm}^3/\text{g}$  when the starch-polymerized aluminum sulfate solution was 10%.

**Author Contributions:** Conceptualization: F.C. and Q.Z.; methodology: F.C.; software: F.C.; validation: Q.Z. and L.Y.; resources: F.C. and L.Y.; writing—original draft preparation: F.C. and L.Y.; writing—review and editing: F.C. and Q.Z.; visualization: F.C. All authors have read and agreed to the published version of the manuscript.

**Funding:** The Key Project of the Natural Science Foundation of Universities in Anhui Province (KJ2021A1389), Anhui Province Outstanding Young Talents Support Program (No. gxyg2021270), Anhui University Collaborative Innovation project (GXXT-2020-057).

**Data Availability Statement:** The data presented in this study are available on request from the corresponding author. The data are not publicly available due to privacy.

**Conflicts of Interest:** The authors declare no conflicts of interests.

## References

1. Zhang, M.; Cao, X.; Li, B.; Zhou, A.T. Quantitative study on the role of desorption gas on coal-gas outbursts: Energy contribution and dynamic characteristics. *Process Saf. Environ.* **2023**, *171*, 437–446. [[CrossRef](#)]
2. Yuan, L.; Jiang, Y.D.; He, X.Q.; Kou, L.M.; Zhao, X.S.; Wang, K.; Yu, Q.; Lu, X.M.; Li, H.C. Research progress in key technologies for accurate identification, monitoring and early warning of typical dynamic disaster risk in coal mines. *J. China. Coal. Soc.* **2018**, *43*, 306–318.
3. Lu, Y.Y.; Zhang, H.D.; Zhou, Z.; Ge, Z.L.; Chen, C.Y.; Hou, Y.D.; Ye, M.L. Current status and effective suggestions for efficient exploitation of coalbed methane in China: A review. *Energy. Fuels* **2021**, *35*, 9102–9123. [[CrossRef](#)]
4. Li, Y.; Wang, Z.S.; Tang, S.H.; Elsworth, D. Re-evaluating adsorbed and free methane content in coal and its ad-and desorption processes analysis. *Chem. Eng. J.* **2022**, *428*, 131946. [[CrossRef](#)]
5. Xi, X.; Jiang, S.J.; Zhang, W.Q.; Wang, K.; Shao, H.; Wu, Z.Y. An experimental study on the effect of ionic liquids on the structure and wetting characteristics of coal. *Fuel* **2019**, *244*, 176–183. [[CrossRef](#)]
6. Wang, Z.; Zhang, S.; Zhang, X.; Li, P.P. Effect of microstructure and chemical composition of coal on methane adsorption. *J. Nat. Gas. Sci. Eng.* **2020**, *82*, 103507. [[CrossRef](#)]
7. Zhao, Y.; Li, M.; Shao, Y. Effect of demineralization on Yimin lignite by experiments and molecular simulation techniques. *J. Mol. Struct.* **2022**, *1269*, 133837. [[CrossRef](#)]
8. Liu, J.X.; Zhong, X.Y.; Jiang, X.M. Solvent Extraction of Superfine Pulverized Coal. Part 2. Free-Radical Characteristics. *Energy Fuels* **2021**, *35*, 15555–15566. [[CrossRef](#)]
9. Zhao, L.; Ni, G.H.; Wang, H.; Sun, Q.; Wang, G.; Jiang, B.Y.; Zhang, C. Molecular structure characterization of lignite treated with ionic liquid via FTIR and XRD spectroscopy. *Fuel* **2020**, *272*, 117705. [[CrossRef](#)]
10. Wang, Z.; Ge, Z.; Li, R.; Liu, X.F.; Wang, H.M.; Gong, S.H. Effects of acid-based fracturing fluids with variable hydrochloric acid contents on the microstructure of bituminous coal: An experimental study. *Energy* **2022**, *244*, 122621.
11. Ren, J.; Wang, Z.; Li, B.; Chen, F.; Liu, J.; Liu, G.; Song, Z. Fractal-Time-Dependent Fick Diffusion Model of Coal Particles Based on Desorption–Diffusion Experiments. *Energy Fuels* **2022**, *36*, 6198–6215. [[CrossRef](#)]
12. Ni, G.; Li, S.; Rahman, S.; Xun, M.; Wang, H.; Xu, Y.H.; Xie, H.C. Effect of nitric acid on the pore structure and fractal characteristics of coal based on the low-temperature nitrogen adsorption method. *Powder. Technol.* **2020**, *367*, 506–516. [[CrossRef](#)]
13. Wang, L.; Liu, M.X.; Zhao, Y.C.; Liao, X.X.; Li, J.; Zhao, Z.; Liu, Q.Q. Multi-scale pore structure transformation of shale under mixed acid acidification method. *Arab. J. Chem.* **2023**, *16*, 104937. [[CrossRef](#)]

14. Yang, Y.; Sun, J.; Li, Z.; Li, J.H.; Zhang, X.Y.; Liu, L.W.; Yan, D.C.; Zhou, Y.B. Influence of soluble organic matter on mechanical properties of coal and occurrence of coal and gas outburst. *Powder. Technol.* **2018**, *332*, 8–17. [[CrossRef](#)]
15. Wang, Z.; Lin, B.; Yang, W.; Li, H.; Lin, M.H. Fracture and pore development law of coal under organic solvent erosion. *Fuel* **2022**, *307*, 121815. [[CrossRef](#)]
16. Ali, M.E.M.; Moniem, S.M.A.; Hemdan, B.A. Innovative polymeric inorganic coagulant-flocculant for wastewater purification with simultaneous microbial reduction in treated effluent and sludge. *S. Afr. J. Chem. Eng.* **2022**, *42*, 127–137. [[CrossRef](#)]
17. Fernandez-Luqueno, F.; Thalasso, F.; Luna-Guido, M.L.; Ceballos-Ramírez, J.M.; Ordoñez-Ruiz, I.M.; Dendooven, L. Flocculant in wastewater affects dynamics of inorganic N and accelerates removal of phenanthrene and anthracene in soil. *J. Environ. Manag.* **2009**, *90*, 2813–2818. [[CrossRef](#)] [[PubMed](#)]
18. Kurniawan, S.B.; Imron, M.F.; Abdullah, S.R.S.; Othman, A.R.; Hasan, H.A. Coagulation-flocculation of aquaculture effluent using biobased flocculant: From artificial to real wastewater optimization by response surface methodology. *J. Water. Process. Eng.* **2023**, *53*, 103869. [[CrossRef](#)]
19. Li, M.; Zhu, X.; Yang, H.; Xie, X.C.; Zhu, Y.T.; Xu, G.Z.; Hu, X.J.; Jin, Z.Y.; Hu, Y.; Hai, Z.B.; et al. Treatment of potato starch wastewater by dual natural flocculants of chitosan and poly-glutamic acid. *J. Clean. Prod.* **2020**, *264*, 121641. [[CrossRef](#)]
20. Hu, P.; Ren, J.; Hu, X.; Yang, H. Comparison of two starch-based flocculants with polyacrylamide for the simultaneous removal of phosphorus and turbidity from simulated and actual wastewater samples in combination with FeCl. *Int. J. Biol. Macromol.* **2021**, *167*, 223–232. [[CrossRef](#)]
21. Ma, Y.F.; Wang, Y.Q.; Zheng, L.; Hou, L.L.; Gao, T.; Jiang, J.J.; Li, L.J. Synthesis of cationic starch flocculant and its performance when treating coal mine wastewater. *Ind. Water Wastewater* **2013**, *44*, 1.
22. Xu, C.; Li, H.; Lu, Y.; Liu, T.; Lu, J.X.; Shi, S.L.; Ye, Q.; Jia, Z.Z.; Wang, Z. Influence of microwave-assisted oxidant stimulation on pore structure and fractal characteristics of bituminous coal based on low-temperature nitrogen adsorption. *Fuel* **2022**, *327*, 125173. [[CrossRef](#)]
23. Chen, Y.; Tang, D.; Xu, H.; Tao, S.; Li, S.; Yang, G.; Yu, J. Pore and fracture characteristics of different rank coals in the eastern margin of the Ordos Basin, China. *J. Nat. Gas. Sci. Eng.* **2015**, *26*, 264–1277. [[CrossRef](#)]
24. Hu, B.; Cheng, Y.; Pan, Z. Classification methods of pore structures in coal: A review and new insight. *J. Nat. Gas. Sci. Eng.* **2023**, *110*, 204876. [[CrossRef](#)]
25. Gao, D.; Guo, L.; Wang, F.; Zhu, L.; Gao, Z. Investigation on thermal analysis and FTIR microscopic characteristics of artificially-oxidized coal and chronic naturally-oxidized coal during secondary oxidation. *Fuel* **2022**, *327*, 125151. [[CrossRef](#)]
26. Chen, C.; Tang, Y.; Guo, X. Comparison of structural characteristics of high-organic-sulfur and low-organic-sulfur coal of various ranks based on FTIR and Raman spectroscopy. *Fuel* **2022**, *310*, 122362. [[CrossRef](#)]
27. Kandagal, V.S.; Pathak, A.; Ayappa, K.G.; Punnathanam, S.N. Adsorption on edge-functionalized bilayer graphene nanoribbons: Assessing the role of functional groups in methane uptake. *J. Phys. Chem. C* **2012**, *116*, 23394–23403. [[CrossRef](#)]
28. Zhang, L.; Kang, T.; Kang, J.; Zhang, X.; Zhang, B.; Guo, J.; Chai, Z. Response of molecular structures and methane adsorption behaviors in coals subjected to cyclical microwave exposure. *ACS Omega* **2021**, *6*, 31566–31577. [[CrossRef](#)]
29. Brunauer, S.; Emmett, P.H.; Teller, E. Adsorption of gases in multimolecular layers. *J. Am. Chem. Soc.* **1938**, *60*, 309–319. [[CrossRef](#)]
30. Rong, L.; Xiao, J.; Wang, X.; Sun, J.; Jia, F.; Chu, M. Low-rank coal drying behaviors under negative pressure: Thermal fragmentation, volume shrinkage and changes in pore structure. *J. Clean. Prod.* **2020**, *272*, 122572. [[CrossRef](#)]
31. Liu, Y.; Ji, X.; Gao, Z.; Wang, Y.; Zhu, Y.; Zhang, Y.; Duan, J. Adsorption characteristics and removal mechanism of malathion in water by high and low temperature calcium-modified water hyacinth-based biochar. *J. Clean. Prod.* **2023**, *411*, 137258. [[CrossRef](#)]
32. Li, A.; Ding, W.L.; He, J.H.; Dai, P.; Yin, S.; Xie, F. Investigation of pore structure and fractal characteristics of organic-rich shale reservoirs: A case study of lower Cambrian Qiongzhusi formation in Malong block of eastern Yunnan Province, South China. *Mar. Pet. Geol.* **2016**, *70*, 46–57. [[CrossRef](#)]
33. Landers, J.; Gor, G.Y.; Neimark, A.V. Density functional theory methods for characterization of porous materials. *Colloid. Surf. A* **2013**, *437*, 3–32. [[CrossRef](#)]
34. He, H.; Liu, P.; Xu, L.; Hao, S.; Qiu, X.; Shan, C.; Zhou, Y. Pore structure representations based on nitrogen adsorption experiments and an FHH fractal model: Case study of the block Z shales in the Ordos Basin, China. *J. Petrol. Sci. Eng.* **2021**, *203*, 108661. [[CrossRef](#)]
35. Lee, J.W.; Hwang, K.J.; Shim, W.G.; Moon, I.S. Thermodynamic and Kinetic Behaviors of Trinitrotoluene Adsorption on Powdered Activated Carbons. *Sep. Sci. Technol.* **2006**, *41*, 3655–3672. [[CrossRef](#)]
36. Zhang, X. Fractal character of coal nanopore and effect of deviation corrected, coal rank, and gas adsorption. *Micropor. Mesopor. Mat.* **2024**, *367*, 112972. [[CrossRef](#)]
37. Zheng, C.; Liu, S.; Xue, S. Effects of chemical solvents on coal pore structural and fractal characteristics: An experimental investigation. *Fuel* **2022**, *327*, 125246. [[CrossRef](#)]
38. Wu, M.; Li, H.; Wang, L.; Yang, X.; Dai, C.; Yang, N.; Li, J.; Wang, Y.; Yu, M.  $\mu$ CT quantitative assessment of the pore-fracture structures and permeability behaviors of long-flame coal treated by infrared rapid heating. *Energy* **2023**, *274*, 127308. [[CrossRef](#)]
39. Yang, L.; Cai, F.; Yuan, Y. Fractal Dimension and Nuclear Magnetic Resonance Characteristics of Surfactants for Coal Gas Desorption. *Fractal Fract.* **2023**, *7*, 217. [[CrossRef](#)]
40. Zhang, J.; Ni, X.; Liu, X.; Su, E. Influences of Different Acid Solutions on Pore Structures and Fractal Features of Coal. *Fractal Fract.* **2024**, *8*, 82. [[CrossRef](#)]

41. Guo, S.; Zhang, L.; Pu, H.; Zheng, Y.; Li, B.; Wu, P.; Qiu, P.; Ma, C.; Feng, Y. Dynamic Compressive Mechanical Property Characteristics and Fractal Dimension Applications of Coal-Bearing Mudstone at Real-Time Temperatures. *Fractal Fract.* **2023**, *7*, 695. [[CrossRef](#)]
42. Sousa-Vieira, M.E.; Fernández-Veiga, M. Efficient Generators of the Generalized Fractional Gaussian Noise and Cauchy Processes. *Fractal Fract.* **2023**, *7*, 455. [[CrossRef](#)]

**Disclaimer/Publisher's Note:** The statements, opinions and data contained in all publications are solely those of the individual author(s) and contributor(s) and not of MDPI and/or the editor(s). MDPI and/or the editor(s) disclaim responsibility for any injury to people or property resulting from any ideas, methods, instructions or products referred to in the content.